# Adsorption modes of Na$^+$ , Li$^+$ , and Mg$^{2+}$ to a model zwitterionic lipid bilayer

Matthew Saunders,[*,†,‡] Abibat Adekoya-Olowofela,[†] Sabrina Downing,[†] and Sagar A. Pandit[*,†]

†*Department of Physics, University of South Florida, Tampa, Florida 33620*

‡*Department of Molecular Biosciences, University of South Florida, Tampa, Florida 33620*

E-mail: mwsaunders@usf.edu; pandit@usf.edu

**Abstract**

The adsorption of ions to soft-porous interfaces plays a critical role in many physical and biological processes, such as the function of electrochemical energy storage devices or the attachment of membrane proteins to cells surfaces. In this work we characterize different adsorption modes, and describe the adsorption behavior of Na$^+$, Li$^+$, and Mg$^{2+}$ onto a porous substrate~~in this context~~. We identify three categories of adsorption based on the degree of dehydration of the ion, viz., steric adsorption corresponding to a lack of dehydration, imperfect adsorption with partial dehydration, and perfect adsorption representing total dehydration. Using 1-palmitoyl-2-oleoyl-sn-glycero-3-phosphatidylcholine (POPC) in salt solution as a generic model system for salt at a soft and porous interface, based on the simulation model used we find that anions, Cl$^-$ , always adsorb sterically ~~, without dehydration~~. Among cations, the divalent Mg$^{2+}$ does not dehydrate, and is also adsorbed sterically. On the other hand, Na$^+$ ~~and Li$^+$~~ adsorbed to a large fraction perfectly ~~with complete dehydration of the ion~~ and Li$^+$ exhibits a significant fraction of imperfectly adsorbed ions,~~In addition, Li$^+$ to a~~

1

~~certain extent exhibits imperfect adsorption characterized by partial dehydration~~. We demonstrate that, with everything else held fixed, the adsorption mode of a cation is determined solely by the strength of the electric field produced by the ion at the distance of the hydration shell.

# 1 Introduction

Interactions of ions with soft, porous, and charge-neutral substrates such as zwitterionic lipid bilayers are important and a common system of interest in soft matter physics and biophysics. Empirical studies towards these use simplified models to interpret observations, e.g. assuming the water as a dielectric continuum, or taking the ions as a spherical entity surrounded by a neatly organized hydration shell.[1]

A simple way of defining adsorption of ions to a substrate comes from the Poission-Boltzmann (PB) theory.[1] This mean-field approximation predicts accumulation of ions near a surface due to the mutual electrostatic repulsion of the ions and entropic factors. ~~This mean-field approximation, due to mutual electrostatic repulsion among the ions and entropic factors, predicts accumulation of ions near a surface.~~ Deviations in ion distribution from the predictions of PB theory near a substrate are the defining characteristic of the specific adsorption phenomenon .[2,3] ~~Often, any deviations in ion distribution, near the substrate, from PB theory are attributed to the specific adsorption phenomenon .[2,3]~~

Experimental studies of ion adsorption can be broadly classified into two main groups – methods that examine the electric field/surface potential produced by the adsorbed ions, e.g, electrophoretic mobility[4] or measurement of the forces between bilayers,[5] and methods that can more directly characterize the location and dynamics of ions such as x-ray or neutron scattering,[6–11] and NMR.[7,12,13]

At the atomistic level, identifying adsorbed ions poses a different kind of challenge. We have addressed this issue previously, where we characterized adsorption by examining the dehydration of ions near the interface.[14–17] This is similar to the kind of adsorption described

by the Langmuir isotherm model, where it is assumed that ions stick to a soft, porous interface through direct interaction.[18] Adsorption defined thusly has been reported in our previous works for monovalent ions such as $Na^+$ and $Li^+$.[14,15,19,20] ~~In this work, we distinguish the specifics of the adsorption of $Na^+$ as opposed to $Li^+$ by the degree of their dehydration.~~ Further, our previous work on divalent ions exhibited that $Mg^{2+}$ maintains its hydration structure regardless of where the ion is located in the lipid bilayer,[14] yet maintaining a distribution distinct from that predicted by PB theory. Hence, in this work we characterize different modes of adsorption corresponding to different ions. Here we~~we feel it is necessary to~~ categorize the adsorption behavior based on degree of dehydration, starting from no dehydration at all as in the case of $Mg^{2+}$ and $Cl^-$, extending to complete dehydration as in the case with $Na^+$. In the somewhat different~~the~~ context of RNA, which is not a soft, porous substrate, the specific binding of ions has been addressed extensively [21–25] based on the mobility of cations and further characterized by models that describe the structure of their coordination shell. Cations bound to RNA are frequently distinguished as being diffuse (similar to our steric adsorbed case), and the site-bound ions are further characterized by outer-shell (again analogous to our steric adsorption ions) or inner shell binding (analogous to the imperfect or perfect adsorbed ions), depending on the folded conformation of the RNA or nearby nucleotides.[21–25]

Along with dehydration, we use specific adsorption in the context of PB density as the defining property of adsorption phenomenon. Based on our previous as well as current atomistic simulations we broadly classify adsorption of ions into three categories – viz. *perfect adsorption*, *imperfect adsorption*, and *steric adsorption*. We also demonstrate that, using different force-field for $Mg^{2+}$ the predominant mode of adsorption of $Mg^{2+}$ to 1-palmitoyl-2-oleoyl-sn-glycero-3-phosphatidylcholine (POPC) is always *steric adsorption*.

# Methods

We perform multiple simulations of POPC bilayers with LiCl and $MgCl_2$ salt. Configurations for each simulation are listed in table 1. Bilayers are constructed of 200 lipids, with 100 lipids per leaflet. Simulations are all performed with 60,000 water molecules to ensure that the simulation box was large enough to have no long-range dipole moment, and have a significant sampling of bulk water. The inclusion of ions substantially increases the region of ordered waters in the system.[14,20] We simulate these systems with a starting concentration of 200 mM salt, in order to ensure that the equilibrium bulk concentration is physiologically relevant and yet statistically viable. Systems with $Mg^{2+}$ are simulated with twice the number of anions to counter the $+2$ charge of the cation. All the ~~new~~ systems are simulated for 1 $\mu$s of simulated time. The $Mg^{2+}$–Li *et al.* system is extended to 2.5 $\mu$s to confirm the long residence time of waters in the first coordination shell of $Mg^{2+}$.[26] It is observed that ions in the bilayer still do not exchange of waters from their first coordination shell, so another 1 $\mu$s simulation is performed using the water-$Mg^{2+}$ interaction model developed by Grotz *et al.* , which significantly increase the water-exchange rate to be closer to the value observed experimentally.[26] All the simulations are performed using the GROMACS molecular dynamics software package, version 5.1.6,[27–31] and analysis is performed using GROMACS built–in analysis tools and in–house software developed on the gromacs API or using the MDanalysis python package.[32–34]

## Bilayer Construction

Lipid bilayers in solvent are constructed by placing POPC lipids on a 10 x 10 grid, and reflecting to create the second bilayer leaflet. 60,000 solvent molecules are then placed into the box above the bilayer grid, with random solvent molecules replaced to add ions (see table 1 for numbers of ions and types in each system). Systems are energy minimized using the steepest-descents algorithm to remove bad-contacts. Following energy-minimization,

both systems are allowed to settle in an NPT dynamic run at a temperature of 250K for 1 ns. Systems are then annealed by heating to 350K, and cooling in steps of 10K to the simulation run temperature of 300K in steps of 155 ps. The final annealed configurations for each system are used as the initial configuration for the production molecular dynamics simulations.

## Molecular dynamics

For total length of simulation runs, see table 1. All systems are simulated with a time step of 4 fs. Neighbor searching is performed every 2 steps. The PME algorithm is used for electrostatic interactions.[35] with a cut-off of 1.6 nm. A reciprocal grid of $56 \times 56 \times 224$ cells is used with 4th order B-spline interpolation. A single cut-off of 1.6 nm is used for Van der Waals interactions. Temperature coupling is imposed with the Nose-Hoover algorithm.[36] Pressure coupling is imposed with the Parrinello-Rahman algorithm.[37]

## Force-field parameters

Lipid-lipid and lipid-water interactions are described using our gromos43a1-s3 model,[38] which is calibrated to work with the SPC/E water model.[39] $Li^+$-water interactions are described using Joung and Cheatham parameters.[40] We use the method described in Saunders *et al.* 2022[20] to compute non-aqueous cross-terms for $Li^+$ (see supporting table S1, and figures S1 and S2 for details). Interactions of $Mg^{2+}$ with water is illusive, consequently there are numerous models developed to describe $Mg^{2+}$ –water interaction.[41–43] These models are optimized to improve the hydration free energies as well as binding energies with various solvent models.[41–43] Previous work by our group has examined $Mg^{2+}$ models from Li *et al.* and Allner *et al.* [41,42] in simulations with POPC lipids,[14] and found little variation among them in terms of their effects on lipid bilayer properties. With this in mind, we chose to focus our work here on the parameters developed by Li *et al.* because their optimization procedures closely follow our focus on binding energies. In recent work it has been reported that the

existing $Mg^{2+}$ parameters, including those developed by Li *et al.* overestimate the residence time for a water molecule in the first coordination shell of an ion.[43] In our past works using this force-field we reported insignificant Langmuir type adsorption of $Mg^{2+}$ ions to the POPC bilayer, with waters retained in the first coordination shell of the ion.[14] We have also performed simulations with the parameters developed by Grotz *et al.* that directly reduce residence times while not significantly changing other solvation properties of the ion.[26,43] This was done to study how the interactions with water could affect the first-shell coordination of $Mg^{2+}$ in the bilayer interface. We have computed~~done this by computing~~ the interaction cross-term for the $Mg^{2+}$ ion from Grotz *et al.* with SPC/E water explicitly, using the Lorentz-Berthelot mixing rules.~~the Lorentz-Berthelot mixing rule and using this without changing the self-term for the $Mg^{2+}$ ion.~~

# Results and Discussion

## Bilayer simulations of Li$^+$ and Mg$^{2+}$

### Lipid bilayer structure

The distribution of electron dense and heavy atoms is often studied by using scattering techniques, like small-angle x-ray and neutron scattering. These methods yield a scattering form-factor. Densities can be obtained from the form-factor by solving the inverse problem, which is a technically hard problem. In experiments this is usually solved by fitting a model to the form-factor. ~~, and by applying a model one can solve the inverse problem to determine the corresponding scattering-length density.~~ Simulations give us direct access to atomic positions, and consequently the densities. This allows us to compute a scattering form-factor by taking a cosine transform of the density. The computed form-factor~~, which~~ can be compared with the direct measurements of the experiment. The simulated lipid bilayer x-ray scattering form-factors and associated electron densities for each system are shown

in figure 1. We compare all form-factors for each system to that of a system simulated without salt, published in our previous work.[15] The bilayer thickness $D_{hh}$ is determined by measuring the distance between the peaks in the electron density, which roughly localize the electron-dense phosphates in the lipid headgroup – the values for this can be seen in table 2.

Experiments often report various types of thicknesses, volumes, and cross-sectional areas that are model dependent. We also compute these quantities to compare the simulation results with experiments. These values are presented in table 2. Based on the $D_{hh}$ and the $2D_C$ there is a slight thickening of the bilayer in the $Li^+$ simulations~~systems~~ above that seen in the $Na^+$ simulation~~system~~. The $Mg^{2+}$ simulations , irrespective of the parameter set, yield ~~report~~ much less thickening than the ~~seen in~~ $Li^+$ simulation.~~, with little variation between the different parameter sets. Turning to the $D_B$, the $Li^+$ systems are significantly thicker than the $Mg^{2+}$ systems, with the least thickened bilayer resulting from the Grotz et al. parameters.~~ The volumes per lipid ($V_L$), headgroup ($V_H$), and chains ($V_C$) are computed using the method of Petrache et al. [44] This is done by optimizing the function:

$$\Omega(v_i) = \sum_{z_j}^{\rho_s} (1 - \sum_{i=1}^{N_{\mathrm{Groups}}} (\rho_i(z_j)v_i)^2), \tag{1}$$

where $\rho_i(z_j)$ is the number density of the $i$ component in the $z_j$ slice of the box and $v_i$ is the corresponding partial component volume. $N_{\mathrm{Groups}}$ is the number of atom groups for which we are dividing the system volume into component volumes – we have groups for solvent plus ions, lipid chain without the terminal methyls ($CH_*$), terminal methyls ($CH_3$), and the lipid headgroups (H). The lipid volumes are then computed as

$$V_C = N_{CH_*} \times v_{CH_*} + N_{CH_3} \times v_{CH_3} \tag{2}$$

and

$$V_H = N_H \times v_{\mathrm{headgroup}}, \tag{3}$$

7

where $N_{\mathrm{CH_*}} = 30$, $N_{\mathrm{CH_3}} = 2$, $N_{\mathrm{H}} = 20$ are the number of united atoms per atom group for CH$_*$, CH$_3$, and H. The chain volume V$_{\mathrm{C}}$ is similar for all systems studied, and there is some variation in the headgroup volume V$_{\mathrm{H}}$. However, this method of dividing up the volume is more prone to errors in the headgroup region due to significant overlap between the headgroup and solvent densities. Thus, we also see similar variation in the total lipid volume V$_{\mathrm{L}}$. ~~which is to be expected - this should be intrinsic to the lipid being studied and not depend on the solution or ion parameter set.~~ The two-dimensional area per lipid A$_{\mathrm{L}}$ is defined as $\frac{2V_c}{2D_c}$ as is often reported from SAXS and SANS experiments,[7] and is an important measure of how the lipids condense as the bilayer thickens.~~$\frac{V_c}{D_c}$. This value is often reported from SAXS and SANS experiments, and is an important measure of how the lipids condense as the bilayer thickens.~~ Both the simulations with Mg$^{2+}$ yield bilayers with a larger A$_{\mathrm{L}}$ than the monovalent ions studied in this work, and are closer in area to the simulation without salt. ~~The Mg$^{2+}$ Li et al. forms a bilayer with an A$_{\mathrm{L}}$ closer that than that of Li$^+$, and the Grotz et al. simulation has a significantly larger A$_{\mathrm{L}}$ than the other systems studied, and much closer to that of the no-salt bilayer.~~

The detailed structure of molecules and their neighborhoods are often studied using various nuclear magnetic resonance (NMR) techniques. ~~Experiments can be performed on lipids labeled with NMR responsive isotopes to quantify the chemical environment of atoms or the organization and dynamics of quadrupole moments.~~ At present, these experiments with various salts are sparse. ~~Much of the available data are of measurements taken using lipids labeled with deuterium at various positions along the molecule, including some headgroup carbons, and the acyl chains. These data are obtained without salt in the system. More data including the effects of salts are needed to validate our simulation results. Further, heavy atom NMR studies are needed to ascertain the environment of lipid headgroups and ions.~~ Thus, we report these data with anticipation that future experiments will fill this gap and validate or invalidate these numbers. Lipid chain ordering is determined via the acyl chain $S_{CD}$ per carbon atom. These can be seen in figure 2.

There is significant increase in chain ordering in the systems with Na$^+$ and Li$^+$, which iswould be consistent with the slight thickening of the bilayer seen in the D$_B$ values. The less coordinated Mg$^{2+}$ systems have remained much closer to the ordering seen in the no-salt simulation.

# Specific ion adsorption

## Bulk ions

Interfaces in salt solutions give rise to a double layer of cations and anions at the surface.[1] Ions in these double layers get stuck to the surface, or adsorb, which is sometimes referred to as specific binding. Zwitterionic lipid bilayers have no net charge before ions are adsorbed, so this adsorption determines the surface charge density on the substrate. This charge is measured experimentally using the electrophoretic mobility of the vesicle. Interpretation of such experiments requires one to define a surface, often called the "slip-surface" where solvent beyond that point can be represented by a dielectric continuum. The electrostatic potential at this surface is the $\zeta$–potential. In simulations the interface is not a simple surface, but a region without a clear point of delineation. ~~Thus, making it difficult to delineate the "slip-surface".~~

### Hydration boundary

~~Thus, w~~We identify~~define~~ this slip-surface boundary as the point where water orientational ordering is negligible, i.e. beyond the "slip-surface" boundary water quadrupoles~~dipoles~~ are sufficiently isotropic, giving dielectric properties of water similar to that of bulk solvent ~~sufficiently randomly oriented~~. We compute this by first dividing the box into slices along the direction normal to the bilayer. For each water within a slice we compute the average value of first and second order legendre polynomial of the cosine of the angle between the box z-axis and the water O-H bond vector, and then average these values over the last 150 ns

of simulated time. Figure 3 shows the water order parameters as a function of the distance of a slice from the bilayer center.

The first order parameter describes the in-out ordering of the bond vector with respect to the box z-axis – a vector parallel to the axis and pointing normal to the bilayer would have a positive ordering, and a vector pointing into the bilayer would have a negative ordering. We see that waters at the surface of each bilayer have a significant outward orientation at the bilayer surface, and that reverses as we move closer to the bilayer center. When compared to the system simulated without ions, we see that the monovalent ions perturb the water in-out orientation more than $Mg^{2+}$, especially in the case of the $Mg^{2+}$–Grotz *et al.* parameters.

The second order parameter roughly describes the organization of the quadrupole moments of water, and the value of this parameter can be used to compute the ~~and the sum over the histogram bins weighted by the number of water in each slice can be related to the~~ quadrupolar splitting values determined in deuterated water NMR experiments.[45,46] The vertical dotted lines in figure 3 denote regions of interest in the bilayer based on the sign ~~directionality~~ of the second order parameter. We call the innermost region of negative ordering $B_{-1}$, which ends when the values become positive. This next region of positive ordering is called $B_{+}$, and the following region of negative ordering is $B_{-2}$. Each bilayer system with ions has these regions, but they are at differing distances from the bilayer center. It should be noted that beyond the $B_{-2}$ region the ordering does not abruptly reach zero in the systems simulated with salt.

Figure 3 shows monovalent ions have less organization in the $B_{-1}$ region (inside the lipid headgroup) when compared to that of the divalent ions, whereas in regions $B_{+}$ and $B_{-2}$ (closer to the bilayer surface) the divalent ions show significantly less organization compared to that of monovalent salts. ~~Again, the monovalent ions have less organized water than the no-salt case, perturbing the water organization when compared to the no-salt simulation. This is distinct from the $Mg^{2+}$ simulations where waters are much more organized than the no-salt case.~~ The hydration boundary is determined by fitting an exponential decay to the

<sub>219</sub> second water order parameter starting at the minimum of the $B_{-2}$ of the histogram. The
<sub>220</sub> decay length is used to demarcate the point where the ordering becomes zero – water beyond
<sub>221</sub> this region is regarded as bulk solvent. The location of the hydration boundary is noted in
<sub>222</sub> figure 3, and the distance to this point from the bilayer center is listed in table 2.

## Poission-Boltzmann Theory

<sub>224</sub> With the boundary defined, we look to the region of bulk solvent to examine the behavior
<sub>225</sub> of ions and ascertain that they follow the predictions of PB-theory.[1] The purpose of this
<sub>226</sub> endeavor is to distinguish the ions in bulk solvent from those that are adsorbed, as the
<sub>227</sub> density of the adsorbed ions are expected to deviate from PB-theory predictions. We must
<sub>228</sub> first compute all the model parameters for the number density and electrostatic potential
<sub>229</sub> predicted by PB-theory, and compare our simulation results to this prediction. The PB-
<sub>230</sub> theory assumes that the number density of ions follow a Boltzmann distribution:

$$\rho(z) = \rho_0 \exp\left(-\bar{z}e\beta\psi(z)\right), \tag{4}$$

<sub>231</sub> where $\rho_0$ is the ion density in the center of the dielectric continuum, $\bar{z}$ is the valency of the
<sub>232</sub> ion, $\beta = (k_bT)^{-1}$, $e$ is the charge on an electron, and $\psi(z)$ is the electrostatic potential. The
<sub>233</sub> surface is defined by the hydration boundary of each system. The lengths of the solvent
<sub>234</sub> occupied regions, $D$, in each system is~~in each of the two systems are~~ found by measuring the
<sub>235</sub> distance across the solvent from the hydration boundary of one leaflet of the bilayer to the
<sub>236</sub> other. These values are listed in table 3. This places the surfaces at $z = \pm D/2$ nm, where
<sub>237</sub> $z = 0$ is the center of the solvent-occupied region of the simulation box. The electrostatic

potential $\psi(z)$ is modeled as a sum between two Debye-Huckle potentials:[1]

$$\psi_1(z) = \psi_s \exp\left(-K(z + \frac{D}{2})\right) \tag{5}$$

$$\psi_2(z) = \psi_s \exp\left(K(z - \frac{D}{2})\right) \tag{6}$$

$$\psi(z) = \psi_1(z) + \psi_2(z) - \big(\psi_1(0) + \psi_2(0)\big), \tag{7}$$

where $\psi_s = \frac{\sigma}{\epsilon_0 \epsilon} K$ is the electrostatic potential at the bilayer surface as defined by the hydration boundary, $\epsilon$ is the dielectric constant of SPC/E water $\epsilon = 70.7$,[47] and $\sigma$ is the surface charge density of the bilayer leaflet.[1]

$\sigma$ is determined for each system by integrating the charge density of all species within the hydration boundary on either side of the bilayer. This charge divided by the box area is the surface charge density. These values can be seen in table 3. Since our phospholipid is zwitterionic, all of the surface charge comes from the ions that have accumulated within the hydration boundary (see figure 4)

Returning to equation 7, $K$ is the inverse Debye length,

$$K = \sqrt{\sum_i \rho_{0,i} \bar{z}_i^2 \frac{e^2}{\epsilon_0 \epsilon k_b T}}, \tag{8}$$

where $\rho_{0,i}$ is the density of each ion in a given system at the center of bulk solvent. This is taken as an average of the number density of each ion in the solvent occupied region of the box.

Finally, we fit equation 4 to the density of anions in bulk solvent via $\rho_0$. The comparisons can be seen in figure 5. Past the hydration boundary of the lipid bilayer, it can be seen that the density of anions continues to climb monotonically. Additionally, the density of cations drops monotonically to a trough value before climbing closer to the bilayer center, near the phosphate groups (see figure 4 and 5).

We also compare the~~other~~ electrostatic potential from our simulations to the potential

<sub>257</sub> from PB-theory (figure 6). The electrostatic potential for each simulated system can be
<sub>258</sub> computed by twice integrating the Poisson equation

$$\phi(z) = -\frac{1}{\epsilon_0} \int_0^z \int_0^{z'} \rho(z) dz dz' + C_1 z + C_2. \tag{9}$$

<sub>259</sub> We set the boundary conditions that the electric field in bulk solvent must be zero, and
<sub>260</sub> the electrostatic potential at the box edge must be zero. The electrostatic potential from
<sub>261</sub> simulation agrees well with the prediction from PB-theory.

## Adsorbed ions

<sub>263</sub>   The total number of adsorbed ions are counted as the number of ions within the "slip-
<sub>264</sub> surface" or "hydration-boundary" of the bilayer, and further characterization is based on
<sub>265</sub> the level of hydration of the ion. Binding constants from the Langmuir Isotherm model are
<sub>266</sub> often computed in experiments to describe ion binding affinity for surfaces; however, this
<sub>267</sub> model requires a fixed number of binding sites per lipid. The actual number of binding sites
<sub>268</sub> per lipid is not known. Therefore, we report the number of ions adsorbed per lipid ($\theta$),
<sub>269</sub> which is related to~~corresponds with~~ the binding affinity of each ion for the lipid bilayer. We
<sub>270</sub> observe 0.51 $Na^+$ per lipid bound, 0.57 $Li^+$ per lipid, 0.13 $Mg^{2+}$ per lipid in the $Mg^{2+}$–Li *et*
<sub>271</sub> *al.* system, and 0.10 $Mg^{2+}$ per lipid in the $Mg^{2+}$–Grotz *et al.* system. We see a substantially
<sub>272</sub> larger number of $Na^+$ and $Li^+$ adsorbed per lipid than $Mg^{2+}$ , which may be reflective of the
<sub>273</sub> amount of space occupied by each ion, and seems to follow the binding modes such that the
<sub>274</sub> more dehydrated ions correlate with a larger number of ions adsorbed per lipid. The fraction
<sub>275</sub> of cations adsorbed in each mode of adsorption can be seen in table 4, and the fractions of
<sub>276</sub> $Cl^-$ anions adsorbed can be seen in supporting table S2~~supporting table ??~~. $Cl^-$ adsorption
<sub>277</sub> fractions follow a similar trend to that of the total number of cations bound, but adsorption
<sub>278</sub> is almost entirely in the steric modality.

## Adsorption modalities

Further characterization of the adsorbed ions begins by examining the first-shell coordination partners of cations in each system. This can be counted by first determining a cutoff value for the first hydration shell of each ion – the values for this cutoff are 3.2 Å for $Na^+$, 2.7 Å for $Li^+$, 3.3 Å for $Mg^{2+}$, and 3.0 Å for $Cl^-$. These values are determined from radial distribution functions for water oxygen (or water hydrogen in the case of $Cl^-$ ) around each. This cutoff is used to produce a neighborlist for ions across each simulation in every frame, and count the number of neighbors within this cutoff. These data areis histogrammed and averaged over the last 150ns of simulation time. The results for this are presented in figure 7.

The number of perfectly adsorbed ions is determined by counting the number of ions without any remaining waters in their first coordination shell. It is observed that in the $Na^+$ system, a majority of the ions adsorbed to the bilayer are completely dehydrated. The $Li^+$ system has a similar fraction of perfectly adsorbed ions compared to $Na^+$, and practically no perfectly adsorbed ions are seen in any of the $Mg^{2+}$ simulations. $Cl^-$ anions are not seen adsorbed perfectly in any simulation.

Similarly to the perfect adsorption case, imperfectly adsorbed ions are counted as ions with one or more waters in their first coordination shell, but missing at least one water from the shell. We use the number of coordinating waters of an ion in the bulk solvent region of our simulation as the maximum coordination number for the ion (Figure 7). This gives a coordination number of 4 for $Li^+$ and 6 for $Mg^{2+}$. We calculate the number of imperfectly adsorbed ionsthis by counting the number of ions with one or more water missing from their hydration shell, and then subtracting the number of perfectly adsorbed ions. We see more than twice the fraction of these ions in the $Li^+$ system compared to the $Na^+$ system. $Mg^{2+}$ shows an insignificant number of imperfectly adsorbed ions. $Cl^-$ adsorbs in a large fraction imperfectly, as they begin to interact with the headgroup trimethylammonium.

The remaining ions are considered sterically adsorbed – this number is whatever ions remain after subtracting the perfect and imperfectly adsorbed ions from the number of

14

overall adsorbed ions based on the position of the hydration boundary. $Mg^{2+}$ seems to have most of the ions in this adsorption mode, where $Na^+$ and $Li^+$ do not adsorb in this way in significant numbers. Additionally, $Cl^-$ shows significant steric adsorption.

These data raise the question, what determines the mode of adsorption for a given ion? Since everything else, such as the substrate and the solvent, are held constant, the magnitude of the electric field at the position of the hydration shell of each ion is all that remains to determine the adsorption modality of the ion (figure 8). The electric field strength of each ion is calculated by applying Coulomb's law to a point charge, placing the test charge at the position of the first hydration shell of the ion in question. We note that the $Mg^{2+}$–Li *et al.* ion keeps waters slightly closer in the hydration shell compared to the $Mg^{2+}$–Grotz *et al.* model, resulting in— thus there is a stronger electric field produced at this point by that ion. The largest ion with the smallest charge-density $Na^+$ dehydrates completely in the largest fraction. $Li^+$ is smaller, and thus the field near the first shell is stronger and can hold waters a little better than $Na^+$ . $Mg^{2+}$ is similar in size to $Li^+$ , but has a 2+ charge and holds onto waters substantially more than either of the monovalent ions. We also note that the $\left\| \vec{E} \right\|$ does not exhibit strong correlation with the fraction of the total number of ions adsorbed in each system, it only determines the adsorption mode.

# Conclusions

Ion adsorption to porous interfaces is a complex interplay between solvent–surface, solvent–ion, and solvent–solvent interactions. With the solvent–surface and solvent–solvent interactions held constant, we identify three different adsorption modalities of ions based on the degree of dehydration of the ion upon adsorption. The binding modality of a particular ion is significantly correlated with the electric field strength of the ion at the position of the first hydration shell, with stronger fields encouraging less dehydration of the ion upon adsorption to the surface (figure 8). This affect appears irrespective of the force-field used in the case of

$Mg^{2+}$, which primarily adsorbs in the non-Langmuir type steric modality. ~~We note that ions that are more hydrated tend to leave the bilayer structure as observed using x-ray scattering relatively unaltered.~~

Furthermore, we identify several bilayer structural parameters that can be verified experimentally via x-ray scattering, neutron scattering, or various NMR methods (figures 1, 2, and 3 respectively). While the effect on lipid bilayer structure is not obvious in the electron density (figure 1), the pertubation can be seen in the $D_B$ and water density – the less hydrated ions induce slight thickening of the lipid bilayer. This is reinforced by the chain ordering, where these ions increase chain ordering (figure 2) while the hydrated ions leave the lipid bilayer structure similar to that of the no-salt case. These two results can be verified experimentally via solvent deuterium NMR, and lipid chain NMR. In the case of POPC, we expect deuterium solvent quadrupolar splitting values will be larger~~smaller~~ for the less hydrated ions $Na^+$ and $Li^+$ when compared to the more hydrated $Mg^{2+}$. (figure 3) We also expect the lipid chain order parameters to follow the opposite trend, with the monovalent ions inducing more ordering and $Mg^{2+}$ inducing a smaller change from the no-salt system. We also expect that the adsorption of $Mg^{2+}$ will be less detectable via the electrophoretic mobility of a vesicle in an MgCl salt solution, as the energy required to remove a hydrated ion from beneath the slip-surface of a vesicle may be low enough to allow their escape, while a dehydrated ion may remain adsorbed. These experiments are needed to verify these conclusions.

# Acknowledgments

# References

(1) Israelachvili, J. N. *Intermolecular and surface forces*; Academic press, 2011.

(2) Stern, O. The theory of the electrolytic double-layer. *Z. Elektrochem* **1924**, *30*, 1014–1020.

(3) Grahame, D. C. The electrical double layer and the theory of electrocapillarity. *Chemical reviews* **1947**, *41*, 441–501.

(4) Smith, M. C.; Crist, R. M.; Clogston, J. D.; McNeil, S. E. Zeta potential: a case study of cationic, anionic, and neutral liposomes. *Analytical and bioanalytical chemistry* **2017**, *409*, 5779–5787.

(5) Marra, J.; Israelachvili, J. Direct measurements of forces between phosphatidylcholine and phosphatidylethanolamine bilayers in aqueous electrolyte solutions. *Biochemistry* **1985**, *24*, 4608–4618.

(6) Fogarty, J. C.; Arjunwadkar, M.; Pandit, S. A.; Pan, J. Atomically detailed lipid bilayer models for the interpretation of small angle neutron and X-ray scattering data. *Biochimica et Biophysica Acta (BBA)-Biomembranes* **2015**, *1848*, 662–672.

(7) Nagle, J. F.; Tristram-Nagle, S. Structure of lipid bilayers. *Biochimica et Biophysica Acta (BBA)-Reviews on Biomembranes* **2000**, *1469*, 159–195.

(8) Pan, J.; Heberle, F. A.; Tristram-Nagle, S.; Szymanski, M.; Koepfinger, M.; Katsaras, J.; Kucerka, N. Molecular structures of fluid phase phosphatidylglycerol bilayers as determined by small angle neutron and X-ray scattering. *Biochimica et Biophysica Acta (BBA)-Biomembranes* **2012**, *1818*, 2135–2148.

(9) Pan, J.; Cheng, X.; Heberle, F. A.; Mostofian, B.; Kucerka, N.; Drazba, P.; Katsaras, J. Interactions between ether phospholipids and cholesterol as determined by scattering

377 and molecular dynamics simulations. *The Journal of Physical Chemistry B* **2012**, *116*, 378 14829–14838.

(10) Uhríková, D.; Kučerka, N.; Teixeira, J.; Gordeliy, V.; Balgavỳ, P. Structural changes in dipalmitoylphosphatidylcholine bilayer promoted by Ca2+ ions: a small-angle neutron scattering study. *Chemistry and physics of lipids* **2008**, *155*, 80–89.

(11) Mason, P.; Ansell, S.; Neilson, G. Neutron diffraction studies of electrolytes in null water: a direct determination of the first hydration zone of ions. *Journal of Physics: Condensed Matter* **2006**, *18*, 8437.

(12) Venable, R. M.; Luo, Y.; Gawrisch, K.; Roux, B.; Pastor, R. W. Simulations of anionic lipid membranes: development of interaction-specific ion parameters and validation using NMR data. *The journal of physical chemistry B* **2013**, *117*, 10183–10192.

(13) Casal, H.; Mantsch, H.; Hauser, H. Infrared and 31P-NMR studies of the interaction of Mg2+ with phosphatidylserines: effect of hydrocarbon chain unsaturation. *Biochimica et Biophysica Acta (BBA)-Biomembranes* **1989**, *982*, 228–236.

(14) Kruczek, J.; Chiu, S.-W.; Varma, S.; Jakobsson, E.; Pandit, S. A. Interactions of Mono-valent and Divalent Cations at Palmitoyl-Oleoyl-Phosphatidylcholine Interface. *Lang-muir* **2019**, *35*, 10522–10532.

(15) Kruczek, J.; Chiu, S.-W.; Jakobsson, E.; Pandit, S. A. Effects of Lithium and Other Monovalent Ions on Palmitoyl Oleoyl Phosphatidylcholine Bilayer. *Langmuir* **2017**, *33*, 1105–1115.

(16) Pandit, S. A.; Bostick, D.; Berkowitz, M. L. Molecular dynamics simulation of a dipalmi-toylphosphatidylcholine bilayer with NaCl. *Biophysical journal* **2003**, *84*, 3743–3750.

(17) Berkowitz, M. L.; Bostick, D. L.; Pandit, S. Aqueous solutions next to phospholipid membrane surfaces: insights from simulations. *Chemical reviews* **2006**, *106*, 1527–1539.

(18) Kalinin, V.; Radke, C. An ion-binding model for ionic surfactant adsorption at aqueous-fluid interfaces. *Colloids and Surfaces A: Physicochemical and Engineering Aspects* **1996**, *114*, 337–350.

(19) Saunders, M.; Steele, M.; Lavigne, W.; Varma, S.; Pandit, S. A. Interaction of salt with ether-and ester-linked phospholipid bilayers. *Biochimica et Biophysica Acta (BBA)-Biomembranes* **2019**, *1861*, 907–915.

(20) Saunders, M.; Wineman-Fisher, V.; Jakobsson, E.; Varma, S.; Pandit, S. A. High-dimensional parameter search method to determine force field mixing terms in molecular simulations. *Langmuir* **2022**, *38*, 2840–2851.

(21) Bowman, J. C.; Lenz, T. K.; Hud, N. V.; Williams, L. D.; others Cations in charge: magnesium ions in RNA folding and catalysis. *Current opinion in structural biology* **2012**, *22*, 262.

(22) Rulíšek, L.; Šponer, J. Outer-shell and inner-shell coordination of phosphate group to hydrated metal ions (Mg2+, Cu2+, Zn2+, Cd2+) in the presence and absence of nucleobase. The role of nonelectrostatic effects. *The Journal of Physical Chemistry B* **2003**, *107*, 1913–1923.

(23) Dudev, T.; Lin; Dudev, M.; Lim, C. First- second shell interactions in metal binding sites in proteins: A PDB survey and DFT/CDM calculations. *Journal of the American Chemical Society* **2003**, *125*, 3168–3180.

(24) Pörschke, D. The mode of Mg++ binding to oligonucleotides. Inner sphere complexes as markers for recognition? *Nucleic Acids Research* **1979**, *6*, 883–898.

(25) Petrov, A. S.; Funseth-Smotzer, J.; Pack, G. R. Computational study of dimethyl phosphate anion and its complexes with water, magnesium, and calcium. *International journal of quantum chemistry* **2005**, *102*, 645–655.

(26) Grotz, K. K.; Cruz-León, S.; Schwierz, N. Optimized magnesium force field parameters for biomolecular simulations with accurate solvation, ion-binding, and water-exchange properties. *Journal of Chemical Theory and Computation* **2021**, *17*, 2530–2540.

(27) Abraham, M. J.; Murtola, T.; Schulz, R.; Páll, S.; Smith, J. C.; Hess, B.; Lindahl, E. GROMACS: High performance molecular simulations through multi-level parallelism from laptops to supercomputers. *SoftwareX* **2015**, *1*, 19–25.

(28) Pall, S.; Abraham, M. J.; Kutzner, C.; Hess, B.; Lindahl, E. Tackling exascale software challenges in molecular dynamics simulations with GROMACS. International Conference on Exascale Applications and Software. 2014; pp 3–27.

(29) Spoel, D. V. D.; Lindahl, E.; Hess, B.; Groenhof, G.; Mark, A.; Berendsen, H. GRO-MACS: fast, flexible, free. *J. Comput. Chem.* **2005**, *26*, 1701.

(30) Lindahl, E.; Hess, B.; Van Der Spoel, D. GROMACS 3.0: a package for molecular simulation and trajectory analysis. *Molecular modeling annual* **2001**, *7*, 306–317.

(31) Berendsen, H. J.; van der Spoel, D.; van Drunen, R. GROMACS: a message-passing parallel molecular dynamics implementation. *Computer Physics Communications* **1995**, *91*, 43–56.

(32) Abraham, M.; van der Spoel, D.; Lindahl, E.; Hess, B. the GROMACS development team GROMACS User Manual version 5.1. 2; 2016. *MJ Abraham, T. Murtola, R. Schulz, S. Páll, JC Smith, B. Hess, E. Lindahl, SoftwareX* **2015**, *1*, 19.

(33) Michaud-Agrawal, N.; Denning, E. J.; Woolf, T. B.; Beckstein, O. MDAnalysis: a toolkit for the analysis of molecular dynamics simulations. *Journal of computational chemistry* **2011**, *32*, 2319–2327.

(34) Gowers, R. J.; Linke, M.; Barnoud, J.; Reddy, T. J. E.; Melo, M. N.; Seyler, S. L.;

Domanski, J.; Dotson, D. L.; Buchoux, S.; Kenney, I. M.; others *MDAnalysis: a Python package for the rapid analysis of molecular dynamics simulations*; 2019.

(35) Essmann, U.; Perera, L.; Berkowitz, M. L.; Darden, T.; Lee, H.; Pedersen, L. G. A smooth particle mesh Ewald method. *The Journal of chemical physics* **1995**, *103*, 8577–8593.

(36) Nosé, S.; Klein, M. Constant pressure molecular dynamics for molecular systems. *Molecular Physics* **1983**, *50*, 1055–1076.

(37) Parrinello, M.; Rahman, A. Polymorphic transitions in single crystals: A new molecular dynamics method. *Journal of Applied physics* **1981**, *52*, 7182–7190.

(38) Chiu, S.-W.; Pandit, S. A.; Scott, H.; Jakobsson, E. An improved united atom force field for simulation of mixed lipid bilayers. *The Journal of Physical Chemistry B* **2009**, *113*, 2748–2763.

(39) Berendsen, H.; Grigera, J.; Straatsma, T. The missing term in effective pair potentials. *Journal of Physical Chemistry* **1987**, *91*, 6269–6271.

(40) Joung, I. S.; Cheatham III, T. E. Determination of alkali and halide monovalent ion parameters for use in explicitly solvated biomolecular simulations. *The journal of physical chemistry B* **2008**, *112*, 9020–9041.

(41) Li, P.; Roberts, B. P.; Chakravorty, D. K.; Merz Jr, K. M. Rational design of particle mesh Ewald compatible Lennard-Jones parameters for+ 2 metal cations in explicit solvent. *Journal of chemical theory and computation* **2013**, *9*, 2733–2748.

(42) Allnér, O.; Nilsson, L.; Villa, A. Magnesium ion–water coordination and exchange in biomolecular simulations. *Journal of chemical theory and computation* **2012**, *8*, 1493–1502.

21

(43) Grotz, K. K.; Schwierz, N. Optimized magnesium force field parameters for biomolecular simulations with accurate solvation, ion-binding, and water-exchange properties in SPC/E, TIP3P-fb, TIP4P/2005, TIP4P-Ew, and TIP4P-D. *Journal of Chemical Theory and Computation* **2021**, *18*, 526–537.

(44) Petrache, H. I.; Feller, S. E.; Nagle, J. F. Determination of component volumes of lipid bilayers from simulations. *Biophysical Journal* **1997**, *72*, 2237–2242.

(45) Åman, K.; Lindahl, E.; Edholm, O.; Håkansson, P.; Westlund, P.-O. Structure and dynamics of interfacial water in an L $\alpha$ phase lipid bilayer from molecular dynamics simulations. *Biophysical journal* **2003**, *84*, 102–115.

(46) Kruczek, J.; Saunders, M.; Khosla, M.; Tu, Y.; Pandit, S. A. Molecular dynamics simulations of ether-and ester-linked phospholipids. *Biochimica et Biophysica Acta (BBA)-Biomembranes* **2017**, *1859*, 2297–2307.

(47) Reddy, M. R.; Berkowitz, M. The dielectric constant of SPC/E water. *Chemical physics letters* **1989**, *155*, 173–176.

(48) Egberts, E.; Berendsen, H. Molecular dynamics simulation of a smectic liquid crystal with atomic detail. *The Journal of chemical physics* **1988**, *89*, 3718–3732.

(49) Douliez, J.-P.; Leonard, A.; Dufourc, E. J. Restatement of order parameters in biomembranes: calculation of CC bond order parameters from CD quadrupolar splittings. *Biophysical journal* **1995**, *68*, 1727.

# Tables and Figures

## Tables

Table 1: Simulation system details. Each simulated system is started with 200 mM salt, and the final bulk concentration is computed from the average number density of ions at the center of the solvent occupied region of the box, from the last 150 ns of simulation time. $Na^+$–Saunders *et al.* simulation trajectories are published in our previous work, and are re-analyzed in this work. The $Mg^{2+}$–Li *et al.* system is extended to 2.5 $\mu$s to ascertain if any exchange of waters from the first shell of $Mg^{2+}$ could be observed. $Li^+$ (a) parameters are obtained from the work by Joung and Chetatham III.[40] $Mg^{2+}$ (b-c) parameters are obtained from Li *et al.* [41] and Grotz *et al.* ,[43] respectively.

| System | No. of Cations | No. of Anions | Starting Bulk Salt Concentration | Final Bulk Salt Concentration | Simulated Time |
|---|---|---|---|---|---|
| $Na^+$ From Saunders *et al.* 2022[20] | 216 | 216 | 200mM | 103mM | 0.7$\mu$s |
| $Li^+$ (a) | 216 | 216 | 200mM | 102.0mM | 1$\mu$s |
| $Mg^{2+}$ (b) | 216 | 432 | 200mM | 152mM | 2.5$\mu$s |
| $Mg^{2+}$ (c) | 216 | 432 | 200mM | 153mM | 1$\mu$s |

Table 2: Bilayer simulation details, and structural parameters. Here we detail the various structural measurements of each simulated bilayer. $D_{hh}$ is the distance measured between the peaks in the electron density, which localize the electron-dense phosphate moiety in the lipid headgroup. $D_B$ is a distance between the Gibb's surfaces[6] on the probability density of solvent as it approaches the lipid bilayer. $2D_C$ is the distance between the Gibb's surfaces on the probability density of lipid chains, and represents the lipid chain thickness. Volume per lipid $V_L$ is measured by dividing the volume of the entire system into solvent and ions, and lipid following the method by Petrache *et al.* [44]. This $V_L$ is the sum of the $V_H$ and $V_C$, which are the volume per lipid headgroup and volume per lipid chains respectively. Area per lipid molecule $A_L$ is computed as the ratio of twice the lipid chain volume $V_C$ with $2D_C$. We also report the position of the hydration boundary of each system, which we compute as the point where the second water order parameter $P_2(cos(\beta)) \approx 0$ as was done in Saunders *et al.* 2019[19].

| | No Salt | Na$^+$ | Li$^+$ | Mg$^{2+}$–Li *et al.* | Mg$^{2+}$–Grotz *et al.* |
|---|---|---|---|---|---|
| $D_{hh}(nm)$ | 3.744 ± 0.107 | 3.764 ± 0.088 | 3.864 ± 0.070 | 3.832 ± 0.364 | 3.768 ± 0.525 |
| $D_B(nm)$ | 3.654 ± 0.047 | 3.936 ± 0.043 | 4.511 ± 0.048 | 4.325 ± 0.044 | 4.213 ± 0.049 |
| $2D_C(nm)$ | 2.707 ± 0.034 | 2.897 ± 0.034 | 3.015 ± 0.034 | 2.880 ± 0.029 | 2.809 ± 0.032 |
| $V_L(\times10^{-3}nm^3)$ | 1215.57 ± 1.0 | 1211.32 ± 1.21 | 1201.2 ± 1.05 | 1219.8 ± 1.24 | 1227.7 ± 1.24 |
| $V_H(\times10^{-3}nm^3)$ | 310.68 ± 1.14 | 314.81 ± 0.75 | 306.0 ± 1.01 | 324.0 ± 1.26 | 327.9 ± 1.10 |
| $V_C(\times10^{-3}nm^3)$ | 904.89 ± 1.28 | 896.50 ± 1.19 | 895.3 ± 0.91 | 895.8 ± 1.05 | 899.8 ± 1.06 |
| $A_L(\times10^{-2}nm^2)$ | 66.86 ± 0.85 | 61.89 ± 0.73 | 59.39 ± 0.69 | 62.21 ± 0.63 | 64.35 ± 0.82 |
| Hydration Boundary (nm) | 2.79 | 3.69 | 3.63 | 3.48 | 3.33 |

Table 3: Poisson-boltzmann theory parameters. These parameters are computed for each simulated system studied (excepting the bulk density ($\rho_{0,i}$), which we fit to our simulation results). These are then used to compute the number density distribution and the electrostatic potential as described by Poisson-Boltzmann theory to compare to our simulation results. $\sigma$ is the surface charge density of the bilayer, D is the length of the bulk-solvent occupied region of the box, K is the Debye screening length, and $\rho_{0,i}$ is the number density of the particular ion at the center of bulk solvent.

| Parameter | Na$^+$ | Li$^+$ | Mg$^{2+}$–Li $et$ $al.$ | Mg$^{2+}$–Grotz $et$ $al.$ |
|---|---|---|---|---|
| $\sigma (e/nm^2)$ | 0.161 | 0.182 | 0.0690 | 0.0476 |
| D $(nm)$ | 26.927 | 26.557 | 26.658 | 25.226 |
| K $(nm^{-1})$ | 3.331 | 3.333 | 3.913 | 3.921 |
| $\rho_{0,cation}$ $(nm^{-3})$ | 0.059 | 0.060 | 0.091 | 0.092 |
| $\rho_{0,anion}$ $(nm^{-3})$ | 0.062 | 0.063 | 0.183 | 0.185 |

Table 4: Fractions per lipid of cations perfectly adsorbed, imperfectly adsorbed, sterically adsorbed, and non-adsorbed cations averaged over the last 150 ns of simulation time. These are computed by counting the number of waters in the first-coordination shell of every ion in the simulation box in every frame. For the total number of adsorbed ions, we only check if the ion is within the hydration boundary of the bilayer. We then subtract the number within this region that are completely dehydrated – these are the perfectly adsorbed ions. We further subtract any ions that have lost one or more waters – the imperfectly adsorbed ions. The remaining are considered sterically adsorbed. ~~We report these numbers as a fraction of ions per lipid of the total number of ions in the system.~~ We also report the total number of bound ions per lipid as a measure of the affinity of the ion to the lipid bilayer – the number of $Mg^{2+}$ ions per lipid is fall smaller than that for the more perfectly adsorbed ions $Li^+$ and $Na^+$.

| Adsorbed cations / lipid | $Na^+$ | $Li^+$ | $Mg^{2+}$–Li *et al.* | $Mg^{2+}$–Grotz *et al.* |
|---|---|---|---|---|
| Total $\theta$ | 0.472~~0.507~~ | 0.575~~0.572~~ | 0.129~~0.117~~ | 0.091~~0.100~~ |
| Steric $\theta_s$ | 0.010~~0.010~~ | 0.015~~0.003~~ | 0.116~~0.093~~ | 0.071~~0.079~~ |
| Imperfect $\theta_I$ | 0.068~~0.066~~ | 0.165~~0.400~~ | 0.008~~0.019~~ | 0.020~~0.021~~ |
| Perfect $\theta_P$ | 0.394~~0.396~~ | 0.395~~0.170~~ | 0.005~~0.005~~ | 0.000~~0.000~~ |

# Figures

Figure 1: Comparison of x-ray scattering formfactors (a,b) and associated electron densities (c,d) for simulated systems. ~~We see little change in the scattering formfactor (a) electron density for the Na$^+$–Saunders *et al.* system (c). Li$^+$ results in a bilayer that is only slightly thickened when compared to the no-salt system.~~ The system with Li$^+$ salt has a slightly thicker bilayer compared to Na$^+$ and the simulation without salt (a,c) and, Mg$^{2+}$ does not significantly change the bilayer thickness under any parameter set studied (b,d).
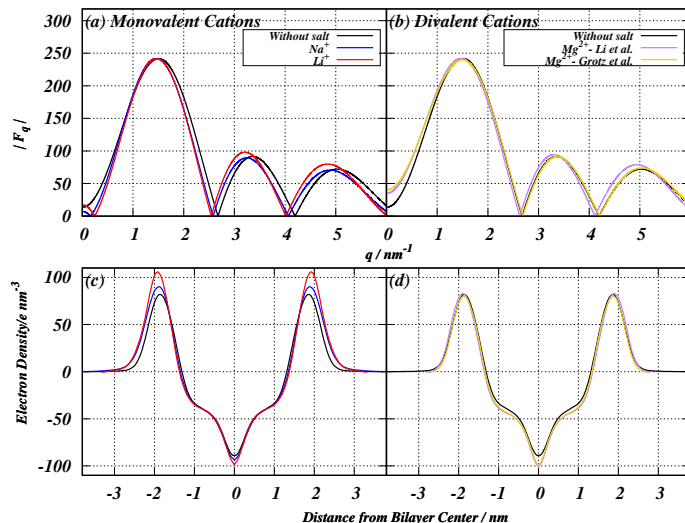
Figure 2: Acyl chain carbon-deuterium order parameters. These are computed for the Sn1 and Sn2 chains of each lipid starting at the second carbon in the chain.[48,49] We note that the lipids simulated in systems of monovalent ions (a,c) show a significant increase in the lipid chain ordering for both acyl chains. The systems simulated with $Mg^{2+}$ (b,d) are much closer in ordering to that of a system simulated without ions.
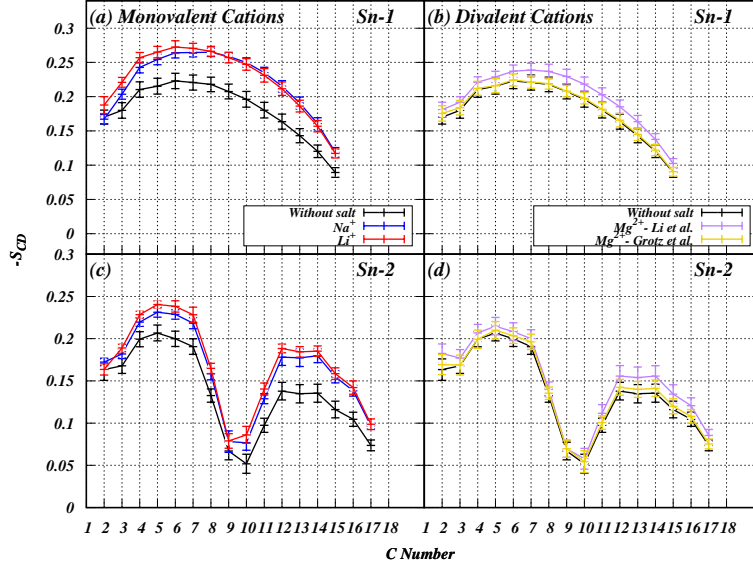
Figure 3: Water order parameters. ~~We see that for the monovalent cations~~ The P1 and P2 calculated for monovalent cations (a,c) show greater organization in the bulk region and the $B_{-2}$ regions, and less organization within the lipid-occupied regions of the system ($B_{+}$ and $B_{-1}$) compared to the simulation without salt. ~~(a,c) there is significantly less organization of the waters in all the systems compared to the no-salt system in both P1 and P2. Na$^+$ and Li$^+$ have similar effects on the water organization in all parts of the lipid bilayer. The Mg$^{2+}$ systems (d) report a much stronger ordering in P2 , with the most organization of the bilayer waters in the Grotz et al. simulation (cyan).~~ On the hand, in the presence of Mg$^{2+}$ salts we observe an overall less pronounced effect in the bulk and $B_{-2}$ regions compared to the system without salt (b,d).
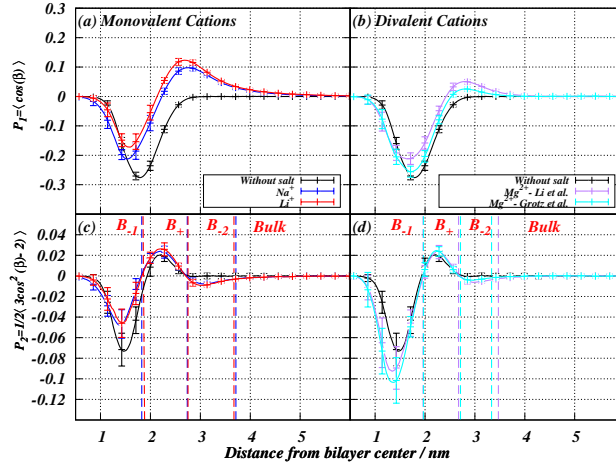
Figure 4: Number density of lipid headgroup species and ions near the bilayer interface. (a-b) We report that the monovalent cations show peaks near the phosphate, with accumulation of an anion peak that resembles the double layer. (c-d) $Mg^{2+}$ does not show significant accumulation in the lipid bilayer headgroup compared to the monovalent ions, with a similarly small anion peak. However, in all systems studied, ions are accumulated near the phosphorus. Integrating the number density of cations within the hydration boundary, denoted by the purple vertical dashed line, gives the number of ions that are sterically bound. The orange vertical dashed line delineates the $D_{hh}$ and the red vertical dashes delineate the $D_C$ of the bilayer.
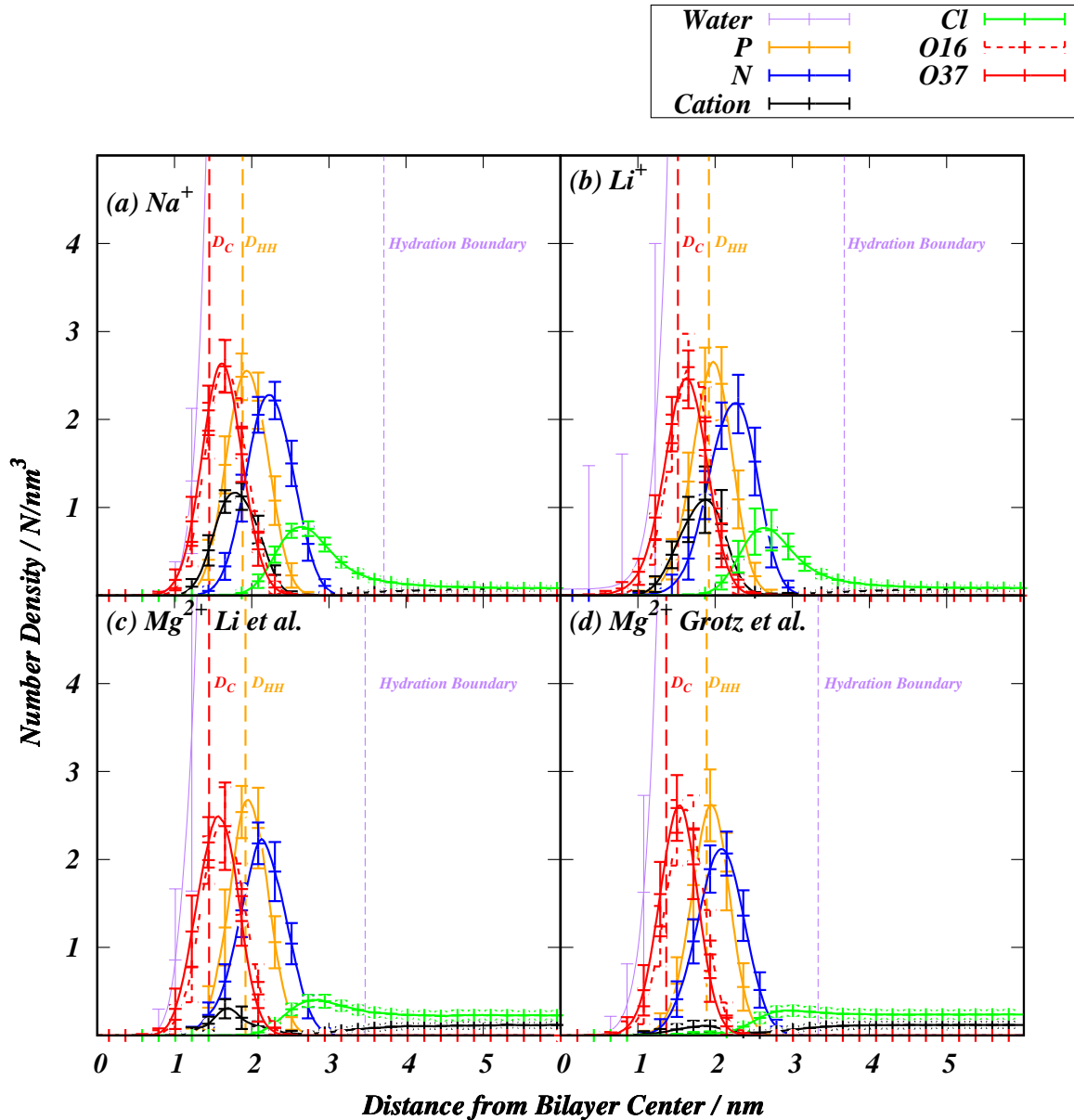
Figure 5: Number density of cations and anions in the bulk solvent-occupied region of each simulated system, compared with theoretical predictions from PB-theory for each calculated $\sigma$. PB-theory predictions correspond well with the simulation results within the region bounded by the hydration boundary.
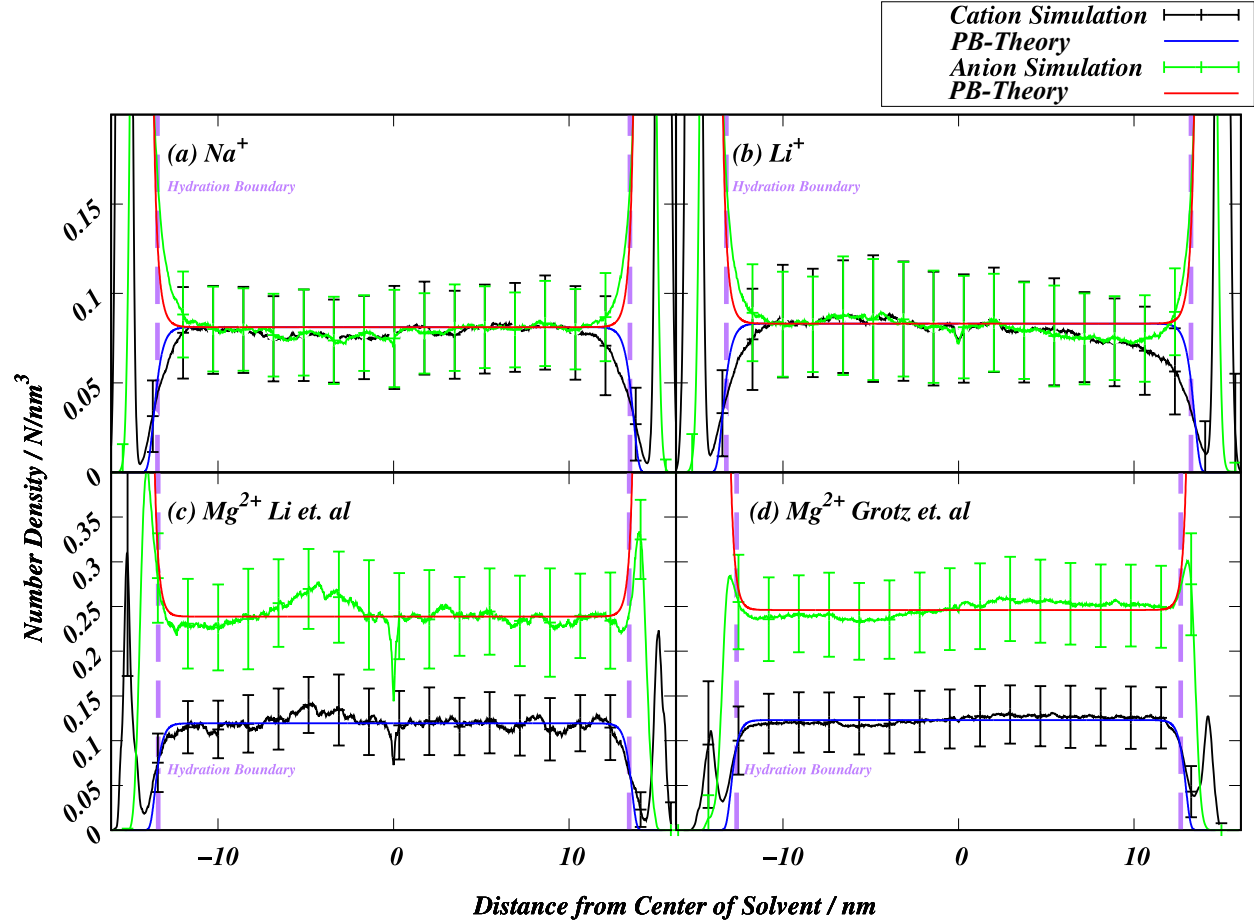
Figure 6: Electrostatic potential in the bulk solvent-occupied region compared to predictions from PB-theory. We report good agreement between the theoretical potential shown in green, and the simulation results shown in black, within the region bounded by the hydration bounds of the lipid bilayer.
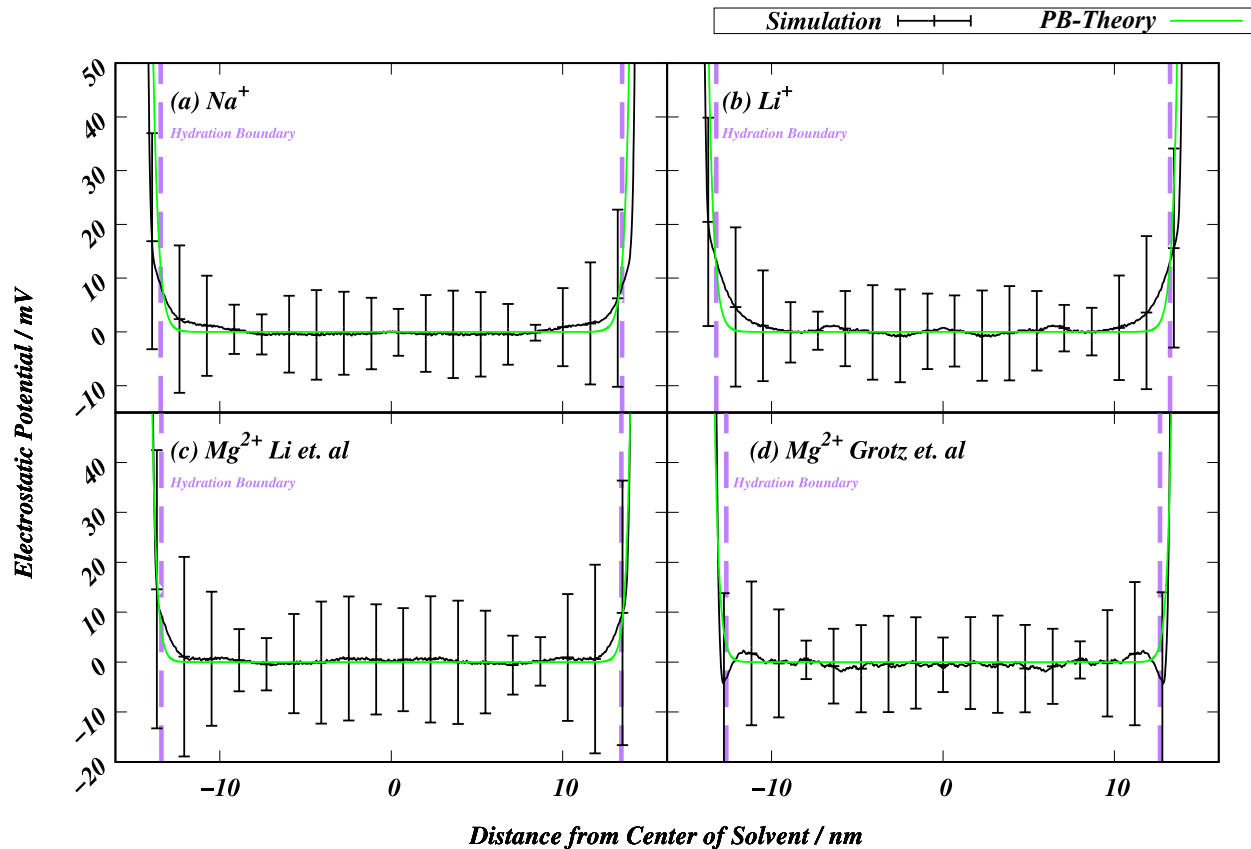
Figure 7: First shell coordination partners for $Li^+$ and $Mg^{2+}$ in each simulation. These are computed over the last 150ns of simulation time in each system by counting the atoms of each species within a cutoff of each ion in the system, and histogramming the data based on the position of the ion. The dotted vertical lines denote the various bilayer surfaces – the vertical black line delineates the hydration boundary of the bilayer, the vertical blue line delineates the $D_{HH}$, and the vertical red line delineates the $D_C$. $Li^+$ (a) retains some water coordination well into the bilayer interface. $Mg^{2+}$–Li *et al.* (b) on the other hand does not lose nearly any first-shell coordinating waters in the bilayer, with some exchange for phosphate oxygens. The $Mg^{2+}$–Grotz *et al.* (c) parameters yield again more exchange but relatively far less than the monovalent ions.
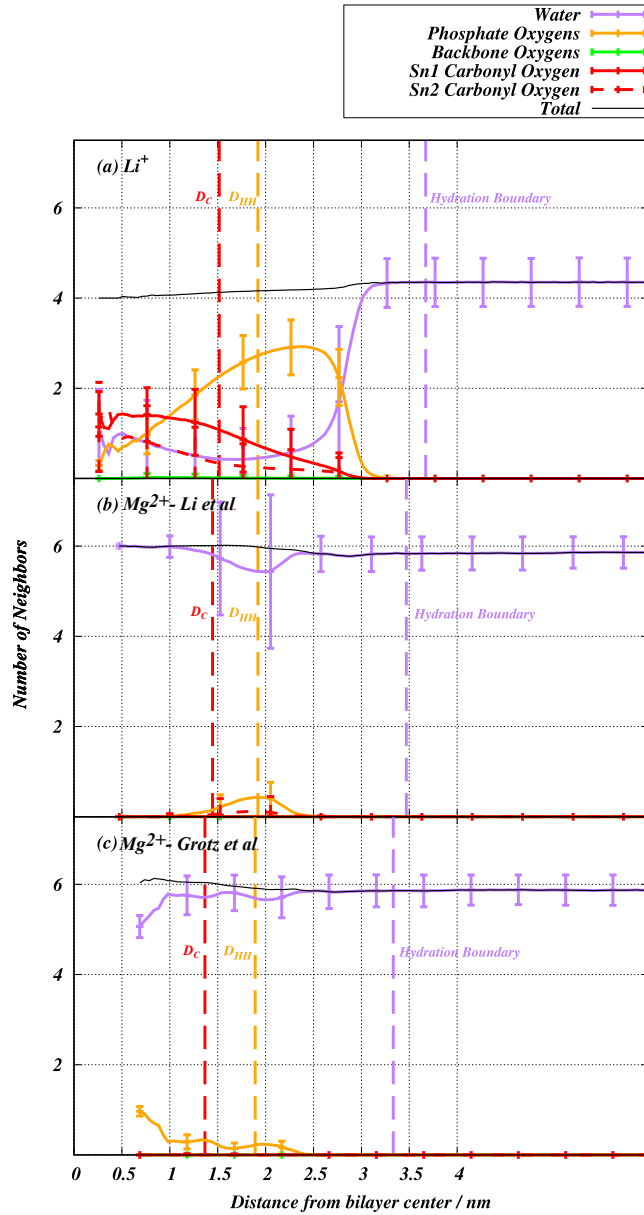
Figure 8: Fractions of ion-adsorption modality per each simulated system as a function of electric field strength. Here we show that the fractions of ions adsorbed in each modality follow a trend with an increasing electric field strength at the hydration shell of the cation. The overall trend is that the cations with the weakest field at the hydration shell position adsorb more perfectly, and as the field strength increases more ions adsorb imperfectly and then sterically. We note that little correlation with field strength can be seen in the total number adsorbed per ion.